Energy Conversion and Management 169 (2018) 186–193

Contents lists available at ScienceDirect

Energy Conversion and Management

journal homepage: www.elsevier.com/locate/enconman

Thermal resistance matching for thermoelectric cooling systems

Xing Lu[a,b,1], Dongliang Zhao[b,1], Ting Ma[a], Qiuwang Wang[a,*], Jintu Fan[c,*], Ronggui Yang[b,*]

[a] Key Laboratory of Thermo-Fluid Science and Engineering, MOE, Xi'an Jiaotong University, Xi'an, Shaanxi 710049, China
[b] Department of Mechanical Engineering, University of Colorado, Boulder, CO 80309, USA
[c] Department of Fiber Science and Apparel Design, College of Human Ecology, Cornell University, Ithaca, NY 14853, USA

ARTICLE INFO

Keywords:
Thermoelectrics
System integration
Thermal resistance matching
Portable cooling

ABSTRACT

The demand of compactness and light-weight for thermoelectric applications requires optimized system integration of thermoelectric module and heat sinks to achieve the best performance under size and weight constraints. This work studies the thermal resistance matching (*i.e.,* optimal thermal resistance allocation of thermoelectric module and heat sinks) for real thermoelectric cooling systems via an integrated theoretical and experimental method. A theoretical model is first developed to study the relationship of thermal resistance allocation and the system cooling power under different operating currents. Modeling results indicate that the optimal thermal resistance of thermoelectric module should account for 40–70% of the total thermal resistance. The effectiveness of thermal resistance matching is then demonstrated in the selection of an optimal thermoelectric module among 73 off-the-shelf modules to develop a portable thermoelectric cooling system. By comparing the cooling performance of two thermoelectric cooling systems with and without thermal resistance matching, it is experimentally demonstrated that the system with thermal resistance matching achieved 10.7–19.8% larger cooling power under the same size and weight constraints. This can be used as a guideline for optimal design of thermoelectric cooling systems.

1. Introduction

Solid-state thermoelectric energy conversion technology that directly converts thermal energy into electric power and vice versa [1] possesses many advantages such as reliability, durability and without environment-unfriendly working fluids [2]. Due to the outstanding merits of compact size, light weight, and fast response, thermoelectric energy conversion is widely used in small and portable systems such as hotspot cooling for electronics [3], laser diode cooling [4], automotive air-conditioner [5], medical applications [6,7] and thermoregulatory clothing system for personal thermal management [8]. However, there is a major disadvantage of thermoelectric energy conversion system, *i.e.*, the low conversion efficiency due to low figure-of-merit of thermoelectric materials [9].

Efforts in improving thermoelectric material performance can potentially lead to the wide-spread application of thermoelectrics [10]. Practical use of thermoelectrics requires addressing challenges not only in the material and module levels, but also in the system level. It has been shown that the system performance is usually much worse than the projected module performance using the intrinsic material properties due to the dependence of the system performance on other components such as heat sinks and thermal interface materials [11]. Thus, for a typical thermoelectric system with hot and cold side heat sinks mounted on the thermoelectric module, the system-level design and optimization is of great importance.

Studies on improving the performance of thermoelectric energy conversion systems have been conducted through theoretical, numerical and experimental methods, or a combination, which generally can be categorized into several groups including optimizing heat sinks, optimizing thermoelectric modules and optimizing the integrated system of thermoelectric module and heat sinks. Theoretical analysis has shown that the finite heat transfer rates of heat sinks have significant influence on the maximum cooling performance of a thermoelectric system [12], and the hot side heat sink has a greater impact on system cooling performance than the cold side [13]. Many efforts have thus been devoted to improving the heat transfer performance of heat sinks including utilizing air-cooled heat sinks with various shapes [14], phase change material-integrated heat sinks [15], thermosyphon heat sinks [16], water jet cooled heat sinks [17] and mini-channel heat sinks [18]. Many earlier studies also focused on the optimization of geometric structures of thermoelectric modules to enhance the cooling capacity. Influence of geometry parameters of thermoelectric elements

* Corresponding authors.
E-mail addresses: wangqw@mail.xjtu.edu.cn (Q. Wang), jf456@cornell.edu (J. Fan), ronggui.yang@colorado.edu (R. Yang).
[1] These authors contributed equally to this work.

https://doi.org/10.1016/j.enconman.2018.05.052
Received 20 February 2018; Received in revised form 14 May 2018; Accepted 15 May 2018

Nomenclature

I	electric current, A
I^*	non-dimensional electric current, $I^* = \alpha_{TE} I/K_{TE}$
I_{max}	maximum electric current, A
K_{TE}	thermal conductance of thermoelectric module, W/K
K^*	non-dimensional thermal conductance of thermoelectric module, $K^* = R_h/K_{TE}{}^{-1}$
P_{blower}	electric power input for blower, W
P_{fan}	electric power input for fan, W
P_{in}	total power input for thermoelectric cooling system, W
P_{TE}	power input for thermoelectric module, W
Q_c	cooling rate, W
$Q_{c,max}$	maximum cooling power for a thermoelectric module, W
Q_h	heat dissipation rate, W
$Q_c{}^*$	non-dimensional cooling rate, $Q_c{}^* = Q_c R_h/T_\infty$
$Q_h{}^*$	non-dimensional heat dissipation rate, $Q_h{}^* = Q_h R_h/T_\infty$
R_c	thermal resistance of cold side heat sink, K/W
R_h	thermal resistance of hot side heat sink, K/W
R_{total}	total thermal resistance of thermoelectric module, hot & cold side heat sinks, K/W
R_{TE}	internal electric resistance of a thermoelectric module, Ω
R^*	non-dimensional thermal resistance of heat sinks, $R^* = R_h/R_c$
T_c	cold side temperature of thermoelectric module, K
$T_c{}^*$	non-dimensional cold side temperature of thermoelectric module, $T_c{}^* = T_c/T_\infty$
T_h	hot side temperature of thermoelectric module, K
$T_h{}^*$	non-dimensional hot side temperature of thermoelectric module, $T_h{}^* = T_h/T_\infty$
$T_{c,out}$	outlet temperature of air in the cold side channel, K
T_∞	ambient temperature, K
ZT	figure-of-merit, $ZT = \alpha_{TE} T/R_{TE} K_{TE}$

Greek symbols

α_{TE}	Seebeck coefficient, V/K
ΔT_{max}	maximum temperature difference of a thermoelectric module, K

Subscripts

c	cold side
h	hot side
max	maximal
n	n-type thermoelectric material
opt	optimal
p	p-type thermoelectric material

on the cooling capacity and the cost benefit has been studied based on analytical method [19,20], genetic algorithm method [21,22] and conjugate-gradient method [23]. Scale effect in terms of different module sizes from bulk module, miniature module to micro module on maximum cooling power was studied by Shen et al. [24]. Novel thermoelectric leg shapes such as cylindrical legs [25] and pyramidal legs [26] are also investigated to improve thermoelectric performance.

In addition to the aforementioned studies on improving performances of heat sinks and thermoelectric modules, there also exist some studies on improving the performance of integrated thermoelectric and heat sink systems. Zhu et al. investigated the optimal size [27] and configuration [28] of hot and cold side heat sinks for thermoelectric cooling systems based on the entropy generation analysis. Zhou et al. [29] and Luo et al. [30] theoretically analyzed the thermal conductance allocation of hot and cold side heat sinks for maximum cooling power under the constraint of a constant total thermal conductance. Lee [31] investigated the optimal ratio of thermal resistance of the hot side heat sink and the thermoelectric module for a thermoelectric power generation system and thermoelectric cooling system assuming that the thermal resistances of hot and cold side heat sinks are the same. Snyder [32] theoretically studied the thermal resistance matching of the heat sinks and the thermoelectric module for a power generation system. The results show that the maximum power output can be achieved when the thermal resistance of the thermoelectric module is equal to the sum of the thermal resistances of the heat sinks at both ends. Apertet et al. [33] found a bell shape relationship of the power output and the thermal conductance of the thermoelectric module under a fixed total thermal conductance of hot side and cold side heat sinks, which indicated that the optimal thermal conductance of thermoelectric module is about equal to the total thermal conductance of the hot side and cold side heat sinks. A higher figure-of-merit of the thermoelectric material does not guarantee a higher power generation without considering the thermal resistance matching. Further analysis by Yazawa et al. [34] found that the maximum output power occurs when the temperature difference across thermoelectric module is exactly half of the total temperature difference across the hot and cold side heat reservoirs when thermal resistances of hot and cold side heat sinks are equal. This idea of thermal resistance matching between the internal thermal resistance of thermoelectric module and the external thermal resistance of heat sinks have been used to guide several later works on the optimization of power output and cost benefits [35–37] for thermoelectric power generation applications.

Similarly, for a thermoelectric cooling system, the performance is not only determined by the thermoelectric modules, but also by the thermal resistance of the hot and the cold side heat sinks. From the above literature review, it can be clearly seen that the thermal resistance matching, *i.e.,* optimal thermal resistance allocation, is particularly important for thermoelectric energy conversion systems. Even

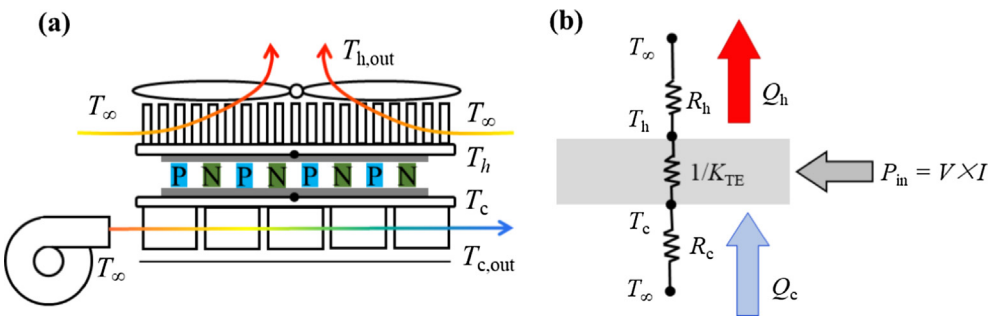

Fig. 1. A thermoelectric cooling system comprises of hot and cold side heat sinks and the thermoelectric module (a) schematic diagram (b) thermal resistance network.

though the wide range of studies on innovative thermoelectric materials, optimization of thermoelectric legs and heat sinks, as well as load matching, can potentially allow full optimization of thermoelectric energy conversion systems, the existing literature lacks guidance for the development of real thermoelectric cooling systems from the perspective of thermal resistance matching by using off-the-shelf thermoelectric modules. This work aims to study the thermal resistance matching of thermoelectric module and heat sinks for a real thermoelectric cooling system via an integrated theoretical and experimental method. A theoretical model is developed first to study the relationship of the thermal resistance allocation of thermoelectric module and heat sinks with the system cooling power. By utilizing the module-level physical parameters extracted from the datasheet of thermoelectric modules, the effectiveness of thermal resistance matching is then demonstrated in the selection of an optimal thermoelectric module among 73 off-the-shelf products to develop a portable thermoelectric cooling system. The improvement of cooling performance is experimentally demonstrated by comparing the performance of two thermoelectric cooling systems with and without optimal thermal resistance allocation.

2. Theoretical model

Fig. 1(a) shows the schematic diagram of a thermoelectric cooling system where two heat sinks are mounted on the hot and cold side of a thermoelectric module. The thermoelectric module is comprised of tens to hundreds of p-n thermocouples connected thermally in parallel and electrically in series where the thermocouples are usually protected by electrically insulated ceramic (covering) substrates. The associated thermal resistance network is shown in Fig. 1(b). Here the thermal resistances of the hot and cold side heat sinks are lumped as R_h and R_c, respectively. The reciprocal of module-level thermal conductance of thermoelectric module, $1/K_{TE}$, is the overall thermal resistance of the thermoelectric module including the thermal resistances of the thermoelectric legs, ceramic plates and copper electrode. We note here that the inclusion of parasitic thermal resistances in $1/K_{TE}$ simplifies the calculation so that there is no need to look into the detailed structure of each thermoelectric module. However, we caution that this method is effective only when the parasitic thermal resistance is small. When operating at an ambient temperature of T_∞, the hot and cold side interface temperatures between the ceramic substrates and heat sink bases, T_h and T_c, are determined by the performance of heat sinks and the thermoelectric module. Note that the temperature difference (T_h - T_c) shown in Fig. 1(b) depends on both thermal resistance ($1/K_{TE}$) of the thermoelectric module and the applied electrical current (I).

For convenience, the dimensionless numbers are defined and used in the theoretical model including: the non-dimensional heat release from the hot side $Q_h^* = Q_h \cdot R_h/T_\infty$, the non-dimensional heat absorption at the cold side $Q_c^* = Q_c \cdot R_h/T_\infty$, the non-dimensional electric current $I^* = \alpha_{TE} \cdot I/K_{TE}$, where I is the operating current applied to the thermoelectric module, the non-dimensional hot side temperature defined as $T_h^* = T_h/T_\infty$, the non-dimensional cold side temperature $T_c^* = T_c/T_\infty$, the non-dimensional ambient temperature $T_\infty^* = 1$, the ratio of the lumped thermal resistance of the hot side and cold side heat sinks $R^* = R_h/R_c$, the ratio of thermal resistances of hot side heat sink and the thermoelectric module $K^* = R_h/(1/K_{TE})$. The thermoelectric figure-of-merit is $ZT_\infty = \alpha_{TE} T_\infty/(R_{TE} K_{TE})$, where α_{TE}, R_{TE} and K_{TE} are the module-level Seebeck coefficient, electric resistance, and thermal conductance of the thermoelectric module, respectively. The present model investigates the thermoelectric cooling systems by using non-dimensional parameters, which enables a clear relationship between the maximum cooling power and a variety of thermal resistance allocations. A general guideline of the optimal thermal resistance allocation that gives maximum cooling power can be obtained and will be discussed in details in Section 4.1.

The non-dimensional heat release from the hot side of a thermoelectric module can be written as:

$$Q_h^* = I^* K^* T_h^* + \frac{1}{2}\frac{I^{*2} K^*}{ZT_\infty} - K^* \cdot (T_h^* - T_c^*) \tag{1}$$

The Q_h^* can also be written as the heat dissipation process through hot side heat sink:

$$Q_h^* = T_h^* - 1 \tag{2}$$

The non-dimensional heat absorption from the cold side of thermoelectric module is:

$$Q_c^* = I^* K^* T_c^* - \frac{1}{2}\frac{I^{*2} K^*}{ZT_\infty} - K^* \cdot (T_h^* - T_c^*) \tag{3}$$

Similarly, the Q_c^* can also be written as the heat absorption process through cold side:

$$Q_c^* = R^* \cdot (T_\infty^* - T_c^*) \tag{4}$$

Solving Eqs. (1)–(4) for Q_c^* by eliminating the non-dimensional temperatures T_h^* and T_c^*, we obtain:

$$Q_c^* = \frac{2K^* \cdot ZT_\infty + I^{*2}K^* + 2I^{*2}K^{*2} - I^{*3}K^{*2} + 2R^* ZT_\infty + 2K^* R^* \cdot ZT_\infty - 2I^* K^* R^* \cdot ZT_\infty}{2ZT_\infty \cdot (K^* + R^* - I^{*2}K^{*2} + I^* K^* + K^* R^* - I^* K^* R^*)} \tag{5}$$

According to Eq. (5), there are four non-dimensional parameters: I^*, ZT_∞, K^*, and R^*. Since the objective of this work is to match thermal resistance of thermoelectric module and thermal resistances of heat sinks, the optimal thermal resistance allocation is calculated by finding a K_{opt}^* which satisfies:

$$\partial Q_c^*/\partial K^* = 0 \tag{6}$$

The optimal electric current, I_{opt}^* to maximize cooling power can be found by solving:

$$\partial Q_c^*/\partial I^* = 0 \tag{7}$$

Thus, the optimal thermal conductance K_{opt}^* under optimal current I_{opt}^* are given by Eqs. (8) and (9), respectively:

$$\frac{(2I^* \cdot K^{*2} - K^* + R^* K^*) \cdot (2K^* \cdot ZT_\infty + 2R^* \cdot ZT_\infty + I^{*2}K^* + 2I^{*2}K^{*2} - I^{*3}K^{*2} + 2K^* R^* ZT_\infty - 2I^* K^* R^* ZT_\infty)}{2ZT_\infty \cdot (K^* + R^* - I^{*2}K^{*2} + I^* K^* + K^* R^* - I^* K^* R^*)^2} - \frac{3I^{*2} \cdot K^{*2} + 4I^* \cdot K^{*2} + 2I^* K^* - 2R^* K^* \cdot ZT_\infty}{2ZT_\infty \cdot (K^* + R^* - I^{*2}K^{*2} + I^* K^* + K^* R^* - I^* K^* R^*)} = 0 \tag{8}$$

$$\frac{(I^* + R^* - 2I^{*2}K^* - I^* R^* + 1) \cdot (2K^* ZT_\infty + 2R^* ZT_\infty + I^{*2}K^* + 2I^{*2}K^{*2} - I^{*3}K^{*2} + 2K^* R^* ZT_\infty - 2I^* K^* R^* ZT_\infty)}{2ZT_\infty (K^* + R^* - I^{*2}K^{*2} + I^* K^* + K^* R^* - I^* K^* R^*)^2} - \frac{2ZT_\infty + 2R^* ZT_\infty + 4I^{*2}K^* - 2I^{*3}K^* + I^{*2} - 2I^* R^* ZT_\infty}{2ZT_\infty (K^* + R^* - I^{*2}K^{*2} + I^* K^* + K^* R^* - I^* K^* R^*)} = 0 \tag{9}$$

By solving Eqs. (8), (9), the optimal variables, K_{opt}^* and I_{opt}^* can be obtained for maximum non-dimensional cooling power, $Q_{c,max}^*$, with respect to R^* and ZT_∞. The solution for K_{opt}^* and I_{opt}^* are numerically solved as implemented in this work and presented in Section 4.1.

3. Module-level property extraction

Most theoretical analysis on thermoelectric energy conversion systems uses physical properties of the p- and n-type thermoelectric materials and the detailed geometrical parameters (leg length, leg cross sectional area and total number of p-n thermocouples etc.) to model the performance. However, for the development of thermoelectric cooling systems using off-the-shelf thermoelectric modules, properties of component materials including the thermoelectric materials, solder, ceramic plates, and the detailed geometry of the module such as thermoelectric leg size and solder layer thickness are not available [38]. It is thus important to design cooling systems with module-level physical

properties which can be extracted using the data sheets from vendors.

Sim et al. [39] provided a method to individually extract the properties of parasitic components (ceramic plates and copper electric) and the properties of the thermoelectric materials based on vendors' datasheets. However, in order to conveniently evaluate and compare a variety of different off-the-shelf thermoelectric modules for system design, lumped module-level physical parameters are employed to quantify the thermoelectric modules regardless of the properties of component materials and the detailed internal geometry of the modules. In this work, we employ an analytical method to obtain the module-level physical properties following Ref. [40]. Table 1 summarizes the extraction of the effective module-level physical properties from vendor's datasheets for off-the-shelf thermoelectric modules including the external dimensions (module length, width and height) as well as cooling performance data ΔT_{max}, $Q_{c,max}$ and I_{max} under controlled hot side temperature T_h. It should be noted that if the parasitic thermal resistance of the non-active parts of the thermoelectric module, such as the ceramic plates, is significant compared to that of the heat sinks and thermoelectric legs, the analytical method proposed by Sim et al. [39] that can individually extract the properties of parasitic components (ceramic plates and copper electric) should be employed. Here, by using Sim's method, we found that the parasitic thermal resistance is only 0.4% - 5.8% compared to the thermal resistance of thermoelectric legs for most of the conventional bulk thermoelectric modules. For simplicity, we decided to include the parasitic resistance in $1/K_{TE}$ for the modeling optimization as described in Section 2.

4. Results and discussion

Section 4.1 shows the relationship of thermal resistance allocation of the thermoelectric module and heat sinks with the system cooling power under different electric currents. Section 4.2 presents the effectiveness of thermal resistance matching in selecting optimal off-the-shelf thermoelectric modules based on their module-level physical properties. Experimental demonstration of the cooling power improvement with thermal resistance matching is presented in Section 4.3.

4.1. Thermal resistance matching for maximum cooling power

As mentioned in Section 2, instead of analytically solving the differential equations Eqs. (8) and (9) for the optimal values of K^*_{opt} and I^*_{opt}, we calculate numerically the relationship of K^*, I^* versus $Q_c{}^*$ to obtain the maximal $Q^*_{c,max}$ values. Here, I^* and K^* are varied from 0 to 1. The input parameter of non-dimensional figure-of-merit is varied from 0.6 to 1.0 based on the state-of-the-art commercial thermoelectric material Bi_2Te_3 and the modules built thereof. The ratio of lumped thermal resistance of hot and cold side heat sinks ranges within 0.1–10, representing a range of diverse heat sink designs.

Fig. 2 shows the relationship between K^*, I^* and $Q_c{}^*$ for several representative cases. As expected, there clearly exists a peak value of $Q_c{}^*$ when K^* and I^* are at their optimal values, K^*_{opt} and I^*_{opt}, for various R^*. The various non-dimensional thermal resistance of heat sinks (ratio of cold side and hot side thermal resistance of heat sinks), R^*, represents diverse heat sink designs under certain constraints such as heat transfer method, size and the weight of heat sinks. When $K^*{}_{opt}$ is determined under a given R^*, the ratios of thermal resistance allocation of the three components, *i.e.*, thermoelectric module, hot side and cold side heat sinks, can be obtained. As the total thermal resistance, R_{total}, is the summation of thermal resistance for the three components as $(1/K_{TE} + R_h + R_c)$, the thermal resistance allocation of the thermoelectric module, $(1/K_{TE})/R_{total}$, the hot side heat sink, R_h/R_{total} and the cold side heat sink, R_c/R_{total} is derived by $R^*/(R^* + K^* + K^*{\cdot}R^*)$%, $K^*{\cdot}R^*/(R^* + K^* + K^*{\cdot}R^*)$% and $K^*/(R^* + K^* + K^*{\cdot}R^*)$%, respectively.

Fig. 3 shows the optimal thermal resistance allocations from the numerical calculations. It can be seen that there is very little difference in the optimal thermal resistance allocation when non-dimensional figure-of-merit is from 0.6, 0.8 to 1.0 under the same R^*. This means that the non-dimensional figure-of-merit has very little effect on $K^*{}_{opt}$. However, the thermal conductance of the thermoelectric module plays an important role in addition to the thermoelectric material figure-of-merit. Different from the thermoelectric figure-of-merit, where the higher the better for thermoelectrics, the thermal conductance (or the thermal resistance) of a thermoelectric module needs to be optimized for given thermal resistances of the heat sinks. If the hot side or cold side heat sink has a large thermal resistance, the thermoelectric module should have small conductance (large thermal resistance) to keep a decent temperature difference across the thermoelectric module. When the hot and cold side heat sinks thermal resistances are small, the thermoelectric module should have a larger conductance (small thermal resistance) to enable a higher cooling power.

According to Fig. 3, the value of $K^*{}_{opt}$ ranges from 0.16 to 0.56 when R^* changes from 0.1 to 10, which suggests that the optimal percentage of thermal resistance of thermoelectric module should account for 40% to 70% of the total thermal resistance in the system. When the hot side thermal resistance is greater than that of the cold side ($R_h > R_c$), the optimal thermal resistance of thermoelectric module should account for 60%-70% of the total thermal resistance of the system. When the hot side thermal resistance of heat sink R_h is equal to that of the cold side, R_c (symmetric heat sink design, $R_h = R_c$), the corresponding optimal percentage of thermal resistance of thermoelectric module should account for about 60% of the total thermal resistance in the system. And if the hot side thermal resistance is smaller than that of the cold side ($R_h < R_c$), the thermal resistance allocation of the thermoelectric module should be reduced from 60% to 40% of the total thermal resistance, which indicates that the thermoelectric module with lower thermal resistance (larger thermal conductance) enables higher heat flow and can be dissipated by a heat sink with better heat dissipation. Since the effect of the hot side thermal resistance is greater than that of the cold side, when the allocation percentage of hot side thermal resistance gets smaller (R_h/R_c decreases from 1 to 0.1), the cooling power increases for a fixed thermoelectric module. To investigate the effectiveness of the thermal resistance matching in a thermoelectric cooling system using commercial off-the-shelf thermoelectric modules, 73 commercially available thermoelectric modules are evaluated and discussed in Section 4.2.

4.2. Evaluation for the off-the-shelf thermoelectric modules

The above non-dimensional analysis provides a general guideline for thermal resistance matching (*i.e.*, optimal thermal resistance of thermoelectric module should account for 40–70% when the ratio of heat sinks R_h/R_c varies from 0.1 to 10). The performance of a thermoelectric cooling system can be readily evaluated by using this thermal resistance matching guideline. In this Section, 73 commercially available off-the-shelf thermoelectric modules are evaluated by utilizing thermal resistance matching idea. Based on our recent work for

Table 1
Module-level physical properties extracted from vendor's datasheets.

Module performance obtained from vendor's datasheets			
Maximum temperature gradient/°C	ΔT_{max}	Maximum cooling power/W	$Q_{c,max}$
maximum electric current/A	I_{max}	hot side temperature/°C	T_h
Module-level physical properties extracted from the vendor's datasheets[38]			
Seebeck coefficient/V·K^{-1}	$\alpha_{TE} = 2\frac{Q_{c,max}}{I_{max}}\frac{1}{T_h - \Delta T_{max}}$		
Electric resistance/Ω	$R_{TE} = 2\frac{Q_{c,max}}{I^2_{max}}$		
Thermal conductance/K·W^{-1}	$K_{TE} = \frac{Q_{c,max}}{\Delta T_{max}}$		
Figure-of-merit based on hot side temperature	$ZT = \frac{2{\cdot}T_h{\cdot}\Delta T_{max}}{(T_h - \Delta T_{max})^2}$		

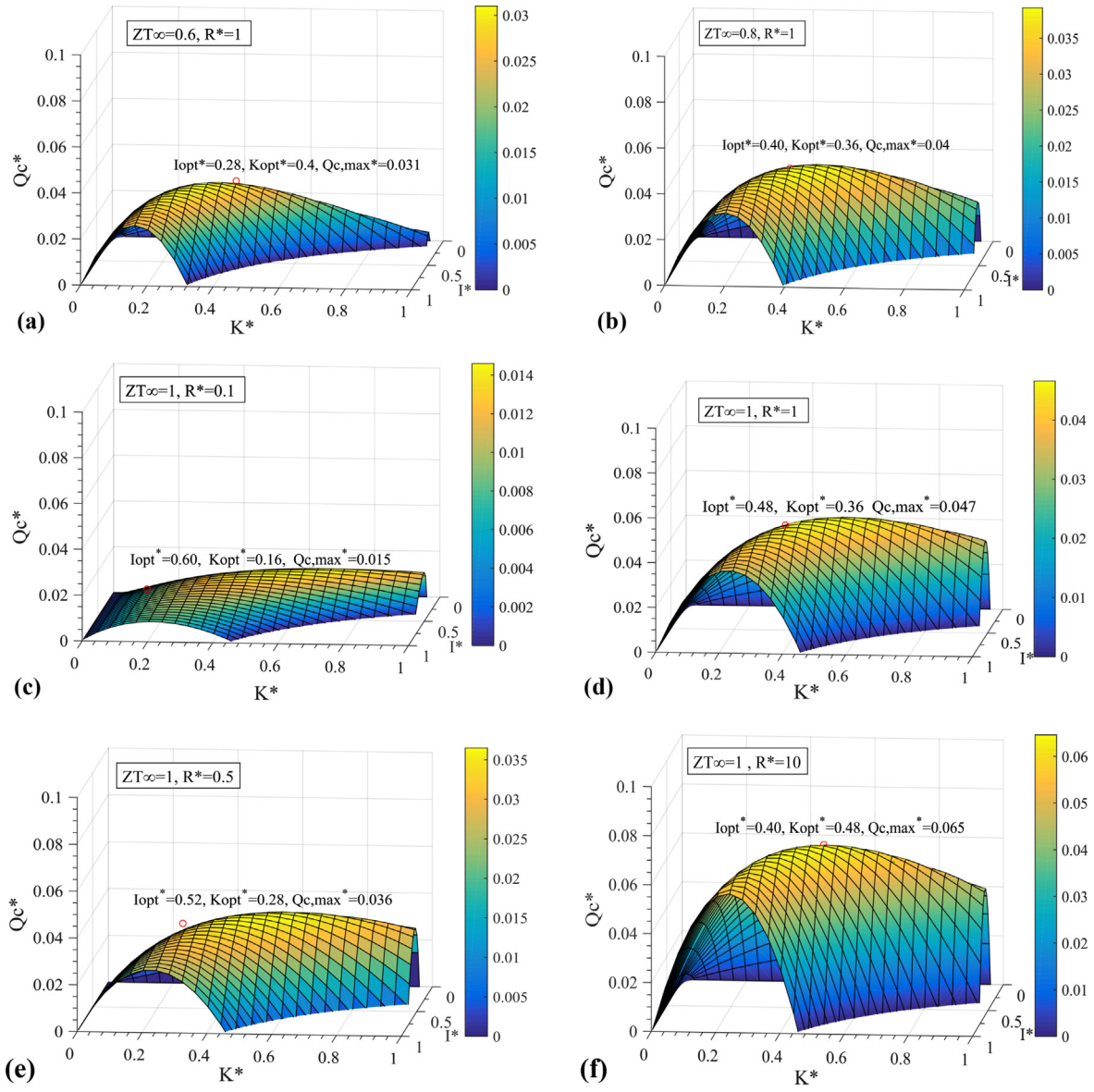

Fig. 2. Relationship between K^*, I^* and Qc^*: (a) $ZT_\infty = 0.6$, $R^* = 1$ (b) $ZT_\infty = 0.8$, $R^* = 1$ (c) $ZT_\infty = 1.0$, $R^* = 0.1$ (d) $ZT_\infty = 1.0$, $R^* = 1$ (e) $ZT_\infty = 1.0$, $R^* = 0.5$ (f) $ZT_\infty = 1.0$, $R^* = 10$.

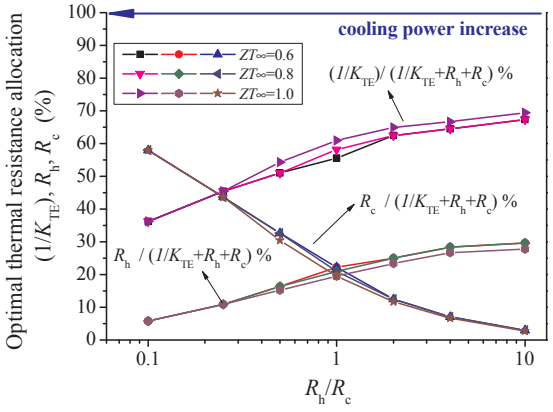

Fig. 3. Optimal thermal resistance allocation versus a variety of heat sink designs (R_h/R_c ranges from 0.1 to 10) with non-dimensional figure-of-merit values (ranges from 0.6 to 1.0).

developing thermoregulatory clothing using portable thermoelectric cooling system, the hot and cold side thermal resistances of air-cooled heat sinks vary within a reasonable range from 0.5 K/W to 2.0 K/W [8].

For room temperature cooling, a wide range of commercial off-the-shelf thermoelectric modules made of bismuth telluride with diverse maximum cooling power from tens to hundreds of watts are available. Here we evaluate 73 off-the-shelf single-stage square shaped thermoelectric modules from three vendors: Laird Technologies [41], CUI Inc. [42] and Marlow Inc. [43]. Table 2 summarizes the nominal cooling capacity and thermal conductance of commercially available Bi_2Te_3-based thermoelectric modules. The module sizes are from 10 mm to 60 mm and the thickness is within 5 mm. The module-level physical properties of the off-the-shelf thermoelectric modules are calculated first according to the procedure described in Section 3. According to Table 1, the relationship of module-level thermal conductance and the module cooling capacity are plotted based on the collected datasheets for these 73 off-the-shelf products. Since the maximum temperature differences are within 65–74 °C, the relationship between K_{TE} and $Q_{c,max}$ suggests an approximately linear relationship because the change of the slope ($1/\Delta T_{max}$) is less than 10%, as shown in Fig. 4.

Fig. 5 shows the maximum cooling powers of the thermoelectric

Table 2
Figure-of-merit, maximum temperature difference, cooling capacity and thermal conductance of off-the-shelf thermoelectric modules with module sizes within 10–60 mm. [41–43]

Module side length (mm)	10–15	20–25	30	40–45	50–60
Maximum temperature difference (°C)	65–74				
Module-level figure-of-merit	0.58–0.88				
Maximum cooling power (W)	3.7–12	18–23	18–95	33–236	80–341
Module-level thermal conductance (W/K)	0.05–0.2	0.13–0.42	0.26–1.4	0.5–3.5	1.2–5

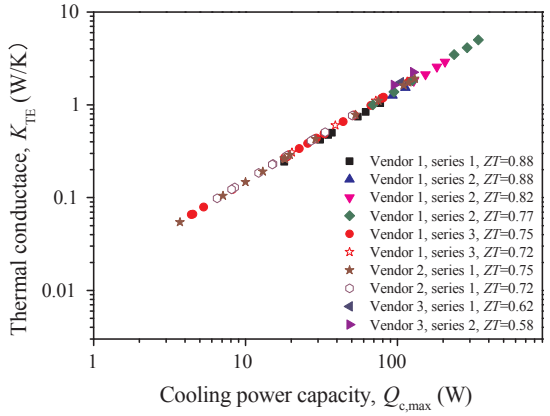

Fig. 4. Relationship of module-level thermal conductance and cooling power capacity of 73 commercial thermoelectric modules with various module-level figure-of-merit values from 0.58 to 0.88.

modules under their optimal currents using various thermal resistances of heat sinks. The reason that the parameters in x-axis and y-axis are converted into real values is to find out the optimal K_{TE} (*i.e.* the thermal resistance matching modules) for thermoelectric cooling systems under given values of R_h and R_c. It can be seen that under constant thermal resistances of heat sinks (R_h, R_c), the thermoelectric module with a higher figure-of-merit provides a larger cooling power when the thermal conductance is kept at the same. When the thermal conductance of a thermoelectric module approaches the optimal value to match the specific heat sinks with given R_h and R_c, the cooling power is maximized. When the thermal conductance of a thermoelectric module does not match to that of the heat sinks, the cooling power decreases even with the increase of the figure-of-merit.

The optimal thermal conductance for a thermoelectric cooling system also depends more on the hot side thermal resistance than on the cold side thermal resistance. For example, by decreasing hot side thermal resistance, R_h, from 2.0 K/W to 0.5 K/W with fixed cold side thermal resistance R_c of 0.5 K/W (shown in Fig. 5(a)), the thermal conductance of the optimal thermoelectric module increase from 0.25 to 0.8 W/K. However, by decreasing cold side thermal resistance, R_c, from 2.0 K/W to 0.5 K/W with constant hot side thermal resistance R_h as 0.5 K/W (shown in Fig. 5(a)-5(c)), the thermal conductance of the optimal thermoelectric module only changes within a small range from 0.4 to 0.5 W/K. The thermal resistance matching of heat sinks and thermoelectric module also indicates the matching between the heat transfer capability of heat sinks (especially the hot side heat dissipation performance) and cooling power capacity of a thermoelectric module.

The above analysis illustrates the importance of thermal resistance matching for the optimal selection of commercial off-the-shelf thermoelectric modules. Since the state-of-the-art thermal conductance of the off-the-shelf thermoelectric modules varies greatly from 0.05 W/K to 5 W/K, the thermal resistance matching should be considered delicately in system design.

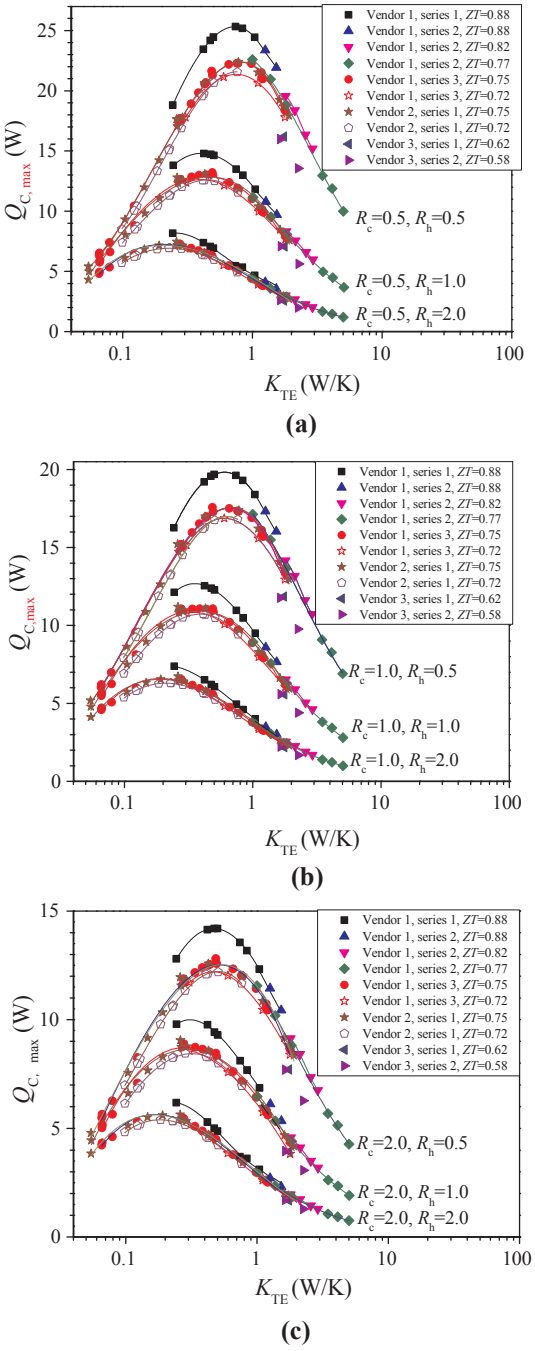

Fig. 5. Maximum cooling power of 73 off-the-shelf thermoelectric modules based on module-level physical properties (within 10–60 mm module side length) at their optimum current with various thermal resistances of heat sinks. (a) Maximum cooling power when R_h varies from 0.5 K/W to 2.0 K/W with R_c equals 0.5 K/W. (b) Maximum cooling power when R_h varies from 0.5 K/W to 2.0 K/W with R_c equals 1.0 K/W. (c) Maximum cooling power when R_h varies from 0.5 K/W to 2.0 K/W with R_c equals 2.0 K/W.

4.3. Experimental demonstration

In this Section, we experimentally demonstrate cooling performance improvement when a portable thermoelectric cooling system is designed with thermal resistance matching. Readers may refer to our previous work [8] for the details on the portable thermoelectric cooling system developed for thermoregulatory clothing application, as shown in Fig. 6. Here, a plate-

fin heat sink is used for the cold side of the thermoelectric cooling system. At the hot-side, a fan-heat sink is employed due to its compactness.

The hot and cold side heat sinks were designed through a weight minimization method in our previous study [8]. The thermal resistances of the cold and hot side heat sinks are 2 K/W and 1 K/W in this experiment, respectively. The hot side thermal resistance is measured by experimental tests and the cold side thermal resistance is provided by the heat sink vendor [44]. In this study, the two heat sinks are kept, but a new thermoelectric module is selected through thermal resistance matching method as articulated in the previous Sections. With the same size and weight constraints, two thermoelectric cooling systems with and without optimal thermal resistance allocation were built for comparison. The two thermoelectric modules are selected according to Fig. 5 (curve of R_c = 2 K/W, R_h = 1 K/W) in Section 4.2: module #1 ($K_{TE,1}$ = 1.05 W/K, ZT = 0.88, accounting for 23% of the total thermal resistance) and module #2 ($K_{TE,2}$ = 0.5 W/K, ZT = 0.88, accounting for 55.6% of the total thermal resistance). It is worth noting that these two thermoelectric modules used for comparison study are from the same series [41]: ZT4,12,F1,4040,TA,W6 (ZT = 0.88) and ZT8,12,F1,4040,TA,W6 (ZT = 0.88). Thus, the material quality can be treated as the same and the only difference is K_{TE}. According to the thermal resistance matching analyzed in Fig. 3, the optimal thermal resistance allocation for the thermoelectric module is around 58% under heat sink thermal resistance ratio of R_h/R_c = 0.5. Thus, the system with thermoelectric module #2 approaches to the optimal thermal resistance allocation and is expected to have larger cooling power.

To demonstrate this, all tests with the two thermoelectric systems are conducted under the same working conditions (e.g. the same blower and fan operating voltage and current). An air flow meter (TSI 4040, accuracy is 2% of reading) is used to measure the air flow rate at the outlet of the cold side. K-type thermocouples (0.2 °C accuracy) are employed to measure cold side air inlet and outlet temperatures. The temperature drop of the cold side air and the net coefficient of performance of the thermoelectric systems are obtained and compared. Here, the temperature drop of the cold side air is calculated by $\Delta T = T_\infty - T_{c,out}$. The net coefficient of performance (COP_{net}) which is defined as ratio of the cooling power ($Q_c = m_c c_p \Delta T$) and total energy consumption including TE module (P_{TE}), blower (P_{blower}) and fan (P_{fan}) is calculated by $COP_{net} = Q_c/(P_{fan} + P_{TE} + P_{blower})$. The experimental uncertainties of the cold side air temperature drop and the coefficient of performance are 5% and 5.7%, respectively.

The cooling performances of the two thermoelectric cooling systems are firstly compared under the same input electric currents, as shown in Fig. 7(a). The temperature drop achieved by the system with thermoelectric module #1 is lower than the one with thermoelectric module #2 for a variety of electric currents. The optimal electric current is 2.8 A for thermoelectric module #1 and 2.2 A for thermoelectric module #2. 5.7 °C of temperature drop at its optimum current ($I_{opt,1}$ = 2.8 A) was achieved for the system with thermoelectric module #1 while 6.6 °C of temperature drop was achieved for the system with thermoelectric module #2 at its optimum current ($I_{opt,2}$ = 2.2 A), which is 16.8% larger than the system with thermoelectric module #1.

The cooling performances of the two thermoelectric cooling systems are also compared under the same input electric power (shown in Fig. 7(b)). The energy consumption of the blower and the fan is 7.8 W and the energy consumption of TE modules is determined by the operating current and voltage. From Fig. 7(b), when the total input electric power is lower than 12 W, the two thermoelectric systems have minor differences in terms of cooling performance. When the input power increases, the temperature drop achieved by the thermoelectric cooling system with module #2 gets larger than that with module #1. To be more specific, (1) if compared at the same total input power condition at around 25 W, the thermoelectric system with module #2 (working at I_2 = 1.9 A) can achieve 10.7% higher temperature drop than that of thermoelectric module #1 (*i.e.*, I_1 = 2.8 A). The COP_{net} is 0.37 for thermoelectric module #2 and 0.34 for thermoelectric module #1, respectively; (2) if compared at the same thermoelectric operating power condition at around 30 W, the system with thermoelectric module #2 is working at its optimal current (*i.e.*, $I_2 = I_{opt,2}$ = 2.2 A), and can achieve 19.8% higher temperature drop than the system with module #1 (working at I_1 = 3.2 A). The COP_{net} is 0.33 for thermoelectric module

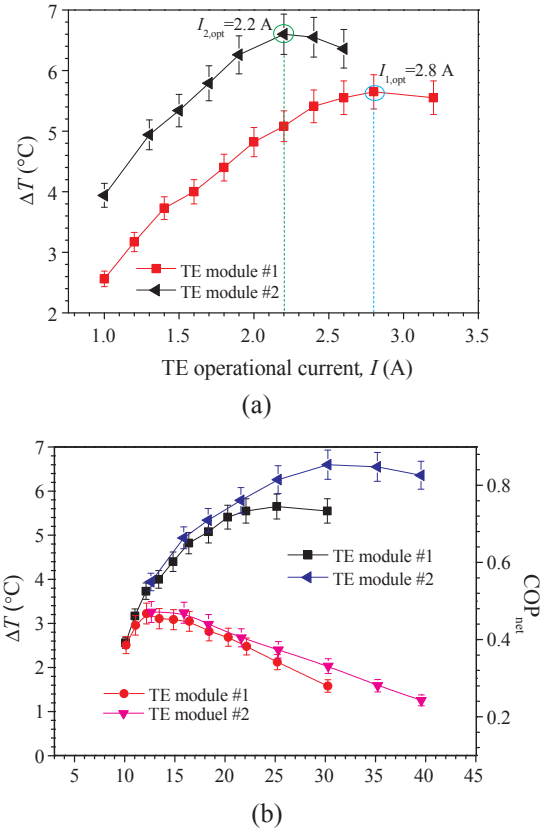

Fig. 7. Cooling performance comparison of the two thermoelectric systems with module #1 and #2. (a) ΔT versus thermoelectric module operational electric current. (b) ΔT and COP_{net} versus total input power.

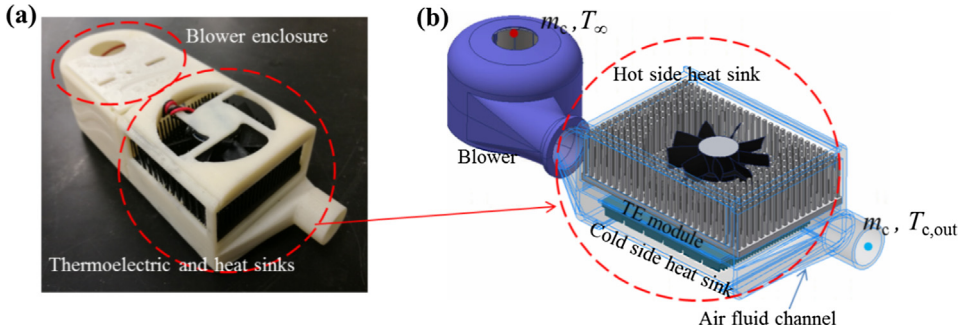

Fig. 6. (a) Photograph and (b) geometric features of the thermoelectric cooling systems tested in this work.

#2 and 0.28 for thermoelectric module #1, respectively. Thus, the experimental study shows that the cooling system achieves 10.7–19.8% larger cooling power due to the thermal resistance matching. This is important for portable thermoelectric cooling systems and can be a guideline for system optimization.

4. Conclusions

Thermal resistance matching is important for thermoelectric energy conversion systems. In this work, a theoretical model is established to study the relationship of thermal resistance allocation (of thermoelectric module and heat sinks) and the system cooling power under different operating electric currents. The theoretical results indicate that the optimal thermal resistance of the thermoelectric module accounts for 40%-70% of the total thermal resistance when the thermal resistance ratio between the hot side and the cold side (R_h/R_c) varies within 0.1–10, which can provide a general guideline for thermal resistance matching of thermoelectric cooling systems. The effectiveness of thermal resistance matching is then demonstrated in selecting an optimal thermoelectric module among 73 off-the-shelf modules to develop a portable thermoelectric cooling system. Experimental demonstration is conducted by comparing the performance of two thermoelectric cooling systems with and without optimal thermal resistance allocation. Results indicate that the thermal resistance matching system can achieve 10.7% to 19.8% larger cooling power.

Acknowledgements

The authors acknowledge the financial support of this work from the US Department of Energy's Advanced Research Projects Agency – Energy (ARPA-E) under contract number DE-AR0000528. X.L. acknowledges the financial support (No. 201606280243) from China Scholarship Council (CSC) for her visit to the University of Colorado, Boulder.

References

[1] Angrist SW. Direct energy conversion. Boston: Allyn and Bacon; 1982. p. 122–9.
[2] Al-Nimr MA, Tashtoush BM, Jaradat AA. Modeling and simulation of thermoelectric device working as a heat pump and an electric generator under Mediterranean climate. Energy 2015;90:1239–50.
[3] Hao X, Peng B, Xie G, Chen Y. Efficient on-chip hotspot removal combined solution of thermoelectric cooler and mini-channel heat sink. Appl Therm Eng 2016;100:170–8. http://dx.doi.org/10.1016/j.applthermaleng.2016.01.131.
[4] Zhang W, Shen L, Yang Y, Chen H. Thermal management for a micro semiconductor laser based on thermoelectric cooling. Appl Therm Eng 2015;90:664–73. http://dx.doi.org/10.1016/j.applthermaleng.2015.07.027.
[5] Attar Alaa, Lee HoSung. Designing and testing the optimum design of automotive air-to-air thermoelectric air conditioner (TEAC) system. Energy Conv Manag 2016;112:328–36.
[6] He RR, Zhong HY, Cai Y, Liu D, Zhao FY. Theoretical and experimental investigations of thermoelectric refrigeration box used for medical service. Procedia Eng 2017;205:1215–22. http://dx.doi.org/10.1016/j.proeng.2017.10.356.
[7] Putra N, Ardiyansyah, Sukyono W, Johansen D, Iskandar FN. The characterization of a cascade thermoelectric cooler in a cryosurgery device. Cryogenics 2010;50:759–64. http://dx.doi.org/10.1016/j.cryogenics.2010.10.002.
[8] Zhao D, Lu X, Fan T, Wu YS, Lou L, Wang Q, et al. Personal thermal management using portable thermoelectrics for potential building energy saving. Appl Energy 2018;218:282–91. http://dx.doi.org/10.1016/j.apenergy.2018.02.158.
[9] Zhao D, Tan G. A review of thermoelectric cooling: materials, modeling and applications. Appl Therm Eng 2014;66:15–24. http://dx.doi.org/10.1016/j.applthermaleng.2014.01.074.
[10] Dresselhaus MS, Chen G, Tang MY, Yang RG, Lee H, Wang DZ, et al. New directions for low dimensional thermoelectric materials (Invited Review). Adv Mater 2007;19:1043–53. http://dx.doi.org/10.1002/adma.200600527.
[11] LeBlanc S. Thermoelectric generators: linking material properties and systems engineering for waste heat recovery applications. Sustain Mater Technol 2014;1:26–35. http://dx.doi.org/10.1016/j.susmat.2014.11.002.
[12] Nagy MJ, Buist RJ. Effect of heat sink design on thermoelectric cooling performance. AIP Conf Proc 1994:147–9. http://dx.doi.org/10.1063/1.46781.
[13] Melnikov AA, Kostishin VG, Alenkov VV. Dimensionless model of a thermoelectric cooling device operating at real heat transfer conditions: maximum cooling capacity mode. J Electron Mater 2017;46(5):2737–44.
[14] Seo YM, Ha MY, Park SH, Lee GH, Kim YS, Park YG. A numerical study on the performance of the thermoelectric module with different heat sink shapes. Appl Therm Eng 2018;128:1082–94. http://dx.doi.org/10.1016/j.applthermaleng.2017.09.097.
[15] Tan G, Zhao D. Study of a thermoelectric space cooling system integrated with phase change material. Appl Therm Eng 2015;86:187–98. http://dx.doi.org/10.1016/j.applthermaleng.2015.04.054.
[16] Araiz M, Martínez A, Astrain D, Aranguren P. Experimental and computational study on thermoelectric generators using thermosyphons with phase change as heat exchangers. Energy Conv Manag 2017;137:155–64. http://dx.doi.org/10.1016/j.enconman.2017.01.046.
[17] Karwa N, Stanley C, Intwala H, Rosengarten G. Development of a low thermal resistance water jet cooled heat sink for thermoelectric refrigerators. Appl Therm Eng 2017;111:1596–602. http://dx.doi.org/10.1016/j.applthermaleng.2016.06.118.
[18] Ahammed N, Asirvatham LG, Wongwises S. Entropy generation analysis of graphene–alumina hybrid nanofluid in multiport minichannel heat exchanger coupled with thermoelectric cooler. Int J Heat Mass Transfer 2016;103:1084–97. http://dx.doi.org/10.1016/j.ijheatmasstransfer.2016.07.070.
[19] Jeong ES. A new approach to optimize thermoelectric cooling modules. Cryogenics 2014;59:38–43. http://dx.doi.org/10.1016/j.cryogenics.2013.12.003.
[20] Pietrzyk Kyle, Ohara Brandon, Watson Thomas, Gee Madison, Avalos Daniel, Lee Hohyun. Thermoelectric module design strategy for solid-state refrigeration. Energy 2016;114:823–32. http://dx.doi.org/10.1016/j.energy.2016.08.058.
[21] Nain PKS, Giri JM, Sharma S, Deb K. Multi-objective performance optimization of thermoelectric coolers using dimensional structural parameters. Swarm Evol Memetic Comput 2010;6464:607–14.
[22] Cheng YH, Lin WK. Geometric optimization of thermoelectric coolers in a confined volume using genetic algorithms. Appl Therm Eng 2005;25:2983–97. http://dx.doi.org/10.1016/j.applthermaleng.2005.03.007.
[23] Huang YX, Wang XD, Cheng CH, Lin DTW. Geometry optimization of thermoelectric coolers using simplified conjugate-gradient method. Energy 2013;59:689–97. http://dx.doi.org/10.1016/j.energy.2013.06.069.
[24] Shen Limei, Huanxin Chen Fu, Xiao Shengwei Wang. The practical performance forecast and analysis of thermoelectric module from macro to micro. Energy Conv Manag 2015;100:23–9.
[25] Ming Tingzhen, Yang Wei, Huang Xiaoming, Yongjia Wu, Li Xiaohua, Liu Jun. Analytical and numerical investigation on a new compact thermoelectric generator. Energy Conv Manag 2017;132:261–71. http://dx.doi.org/10.1016/j.enconman.2016.11.043.
[26] Fabián-Mijangos A, Gao M, Alvarez-Quintana J. Enhanced performance thermoelectric module having asymmetrical legs. Energy Conv Manag 2017;148:1372–81. http://dx.doi.org/10.1016/j.enconman.2017.06.087.
[27] Zhu L, Tan H, Yu J. Analysis on optimal heat exchanger size of thermoelectric cooler for electronic cooling applications. Energy Conv Manag 2013;76:685–90. http://dx.doi.org/10.1016/j.enconman.2013.08.014.
[28] Zhu L, Yu J. Optimization of heat sink of thermoelectric cooler using entropy generation analysis. Int J Therm Sci 2017;118:168–75. http://dx.doi.org/10.1016/j.ijthermalsci.2017.04.015.
[29] Zhou Y, Yu J. Design optimization of thermoelectric cooling systems for applications in electronic devices. Int J Refrig 2012;35:1139–44. http://dx.doi.org/10.1016/j.ijrefrig.2011.12.003.
[30] Luo Y, Zhang L, Li J, Li C, Xie L, Liu Z, et al. Study on thermal conductance allocation ratio of heat sink of thermoelectric cooler for electronic device in cold region. Energy Procedia 2015;75:603–7. http://dx.doi.org/10.1016/j.egypro.2015.07.464.
[31] Lee HS. Optimal design of thermoelectric devices with dimensional analysis. Appl Energy 2013;106:79–88. http://dx.doi.org/10.1016/j.apenergy.2013.01.052.
[32] Snyder GJ, in: Priya S, Inman DJ, editors, Thermoelectric energy harvesting, energy harvesting technologies. Springer; 2009 (chapter 11).
[33] Apertet Y, Ouerdane H, Glavatskaya O, Goupil C, Lecoeur P. Optimal working conditions for thermoelectric generators with realistic thermal coupling. Europhys Lett 2012;97:28001.
[34] Yazawa K, Shakouri A. Optimization of power and efficiency of thermoelectric devices with asymmetric thermal contacts. J Appl Phys 2012;111:024509. http://dx.doi.org/10.1063/1.3679544.
[35] Mayer PM, Ram RJ. Optimization of heat sink-limited thermoelectric generators. Nanoscale Microscale Thermophys Eng 2006;10:143–55. http://dx.doi.org/10.1080/10893950600643063.
[36] Leonov V, Fiorini P, Vullers RJM. Theory and simulation of a thermally matched micromachined thermopile in a wearable energy harvester. Microelectron J 2011;42:579–84. http://dx.doi.org/10.1016/j.mejo.2010.08.002.
[37] Rezania A, Yazawa K, Rosendahl LA, Shakouri A. Co-optimized design of microchannel heat exchangers and thermoelectric generators. Int J Therm Sci 2013;72:73–81. http://dx.doi.org/10.1016/j.ijthermalsci.2013.05.002.
[38] Lee H, Sharp J, Stokes D, Pearson M, Priya S. Modeling and analysis of the effect of thermal losses on thermoelectric generator performance using effective properties. Appl Energy 2018;211:987–96. http://dx.doi.org/10.1016/j.apenergy.2017.11.096.
[39] Sim M, Park H, Kim S. Modeling and extraction of parasitic thermal conductance and intrinsic model parameters of thermoelectric modules. J Electron Mater 2015;44:4473–81. http://dx.doi.org/10.1007/s11664-015-3985-0.
[40] Chen M, Jeffrey Snyder J. Analytical and numerical parameter extraction for compact modeling of thermoelectric coolers. Int J Heat Mass Transf 2013;60:689–99. http://dx.doi.org/10.1016/j.ijheatmasstransfer.2013.01.020.
[41] Laird Technologies. <https://www.lairdtech.com/product-categories/thermal-management/thermoelectric-modules>.
[42] CUI Inc. <http://www.cui.com/catalog/thermal-management/peltier-devices>.
[43] Marlow Inc. <http://www.marlow.com/thermoelectric-coolers.html>.
[44] Alpha Novatech. https://www.alphanovatech.com/en/c_z50e.html.